Original Article

A method for estimating superplastic material parameters via free–inflation tests

Luis García-Barrachina [a,], Donato Sorgente [b], Luigi Tricarico [c], Antonio J. Gámez [a]*

[a] *Dept. of Mechanical Engineering and Industrial Design, School of Engineering University of Cadiz, Av. Universidad de Cádiz, 10, Puerto Real, Cádiz, 11519 Spain*
[b] *School of Engineering, Universitá Degli Studi Della Basilicata, Via Ateneo Lucano, 10-85100, Potenza, Italy*
[c] *Dipartimento di Meccanica, Matematica e Management, Politecnico di Bari, Viale Japigia 182, 70126, Bari, Italy*

ARTICLE INFO

ABSTRACT

In this work, a new methodology for evaluating the constitutive parameters of superplastic materials is presented. The proposed methodology provides the characterization of the material by means of a variable called apparent viscosity. This variable is calculated for three different materials through data collected by free inflation tests made at different temperatures and pressure values. The apparent viscosity was then used to calculate some material parameters by which the experimental tests were reproduced numerically in a finite element commercial code. The results obtained by numerical simulations were compared both with the experimental ones and with ones deriving by simulations run with material parameters calculated by a commonly used methodology. The proposed approach revealed to have a good prediction capability with deviations lower than the one found by the approach taken as reference. A second validation step was then performed by comparing the stress and strain-rate values found through the proposed methodology with the curves constructed by applying uniaxial tests results from literature. This latter comparison showed that results fit well with the behaviour shown using the standardised uniaxial tests.

1. Introduction

Superplastic forming (SPF) is a deforming process that is mainly applied to shell-like pieces to produce complex shapes [1]. SPF relies on the capacity of certain materials to reach extraordinary levels of deformation under particular conditions [2].

The correct outcome of a SPF process requires the adjustment of all the geometrical and physical variables that take part in it as well as the initial conditions of the material in terms of initial microstructure [3].

Traditionally, the study and research of superplastic forming processes have been supported by disparate laboratory-scale tests like cap shapes [4], cap shapes with moving male-die [5], conical shapes [6], cylindrical shapes [7], more complex shapes including stiffeners in two directions [8] or free-inflation tests [9]. This disparity has tended to a biaxial characteristic test versus the uniaxial test normally used to characterise the material.

The biaxial tests promote a state of biaxial tension on the material and is usually achieved by applying a deformation on the two preferential axes of the sample. To achieve this deformation, a restriction of the displacement at certain points and the application of a normal load to the surface are required. This deformation can be achieved by mechanical action from a male mould [10] or by an external pressure generated by an inert gas [11].

Inside the latter group there are two categories: one which takes strain-rate as the target variable to be followed [12], therefore requiring a previous study using some algorithmic operation [4,6,7,13] to obtain the history of pressure to be applied, and another in which a constant pressure is applied [14].

The free-inflation test [15] is a type of biaxial test in which a specimen, which is usually anchored in its perimeter, is allowed to expand freely within a cylindrical die. In this configuration, the only interaction with the mould is restricted to the entry radius that is normally in the order of 10% of the die radius.

In the last decade, much attention has been paid to this kind of test for different purposes:

- to evaluate the working conditions for SPF in terms of pressure and temperature [16].
- to characterise materials [17–19].
- to evaluate behavioural laws [14,20,21].
- to study the behaviour of the microstructure [22].

There is a standard based on the biaxial test, ASTM E2712-15 [23], which aims to evaluate whether a sheet of a certain thickness will be able to withstand a forming process of a certain depth, as well as to study the cavitation process during forming. Unfortunately, and according to the standard itself, it could only be used with success in aluminium alloys and their use in titanium or magnesium alloys has to be yet verified.

Compared to the tensile test, the biaxial test has certain advantages:

- its stress state is more similar to that of a real part
- samples are easier to manufacture
- if the test is carried out at constant pressure, its initial configuration is simplified

Similarly, there are also certain disadvantages that must be taken into account:

- it is a non-standardised process for characterising the material
- an additional system is needed to provide and control the gas supply
- an additional system is needed to record the progress of the test

Given the simplicity of the free-inflation test, numerous studies have emerged to develop also a mathematical approach to the problem. This type of work is focused on obtaining models that could be used in the prediction of the main output variables such as forming time or thickness distribution [24–26]. The different models make use of equilibrium, compatibility and the constitutive equations with greater or lesser approximation, to then integrate them and obtain the expressions, usually implicitly, of the height evolution, thickness distribution or the thickness at a certain point as a function of time.

In the same way, other works [27] have made use of free-inflation test to calculate the material parameters from an analytical approach. More recently, computer methods have been used in order to calculate the material behaviour via free-inflation test. Thus, comparing both numerical and experimental results, the algorithm can lead towards the correct set of material parameters [9,28].

In that sense, the aim of this work is to propose a new method to systematically obtain the parameters of any material under a superplastic behaviour via free-inflation tests. This method does not require the support of finite-element simulations and provides the characterisation of the material by a new variable called apparent viscosity that can be linked to the material parameters. The method is evaluated in three ways: comparing the values of the parameters with the method proposed in [27], comparing the values of experimental forming time with the simulated ones using the obtained parameters, and applying the method to works in the literature that provide both material characterisation via tensile tests and free-inflation experiments.

2. Methodology

2.1. Theoretical framework

The behaviour of superplastic materials, since they are strongly strain rate dependent, can be described by tracing a stress versus strain rate plot. This plot has been historically modelled by several mathematical functions that cover the behaviour in different strain-rate ranges and phenomena, such as strain hardening or material recrystallization. A summary of these functions can be found in [29]. The simplest mathematical expression that models superplastic behaviour is a power-law function as

$$\sigma = K\dot{\varepsilon}^m \tag{1}$$

where the stress σ is related to the strain rate $\dot{\varepsilon}$ via two material parameters K and m, representing a straight line in logarithmic scale with m as the slope.

Normally, the existing methods that characterise superplastic materials aim to find the K and m parameters [9,11,26,28] from the power-law function.

The methodology presented here lies on the idea that the material in superplastic conditions behaves as a strain-rate dependent non-newtonian fluid [6,7]. In this sense, the characterisation of the material needs to provide a fluid-like variable called apparent viscosity μ_a, which relates the strain-rate and the stress in the form

$$\sigma = \mu_a \dot{\varepsilon} \tag{2}$$

meaning that the apparent viscosity can be written using the habitual parameters as

$$\mu_a = K\dot{\varepsilon}^{m-1} \tag{3}$$

In order to calculate the apparent viscosity associated to the material, we start by performing a free-inflation test on a sheet with initial thickness s_o and die radius l_o, therefore characterising the slenderness of the sheet by the Aspect Ratio, $AR = l_o/s_o$, Fig. 1. From [24], the stress can be calculated as

$$\sigma = AR\frac{q_o}{4}f(H) = \frac{l_o}{s_o}\frac{q_o}{4}\frac{\left(1+H^2\right)^2}{H} \tag{4}$$

where its evolution is found to be a function of the dimensionless height, $H = h/l_o$, and the constant external pressure, q_o. Eq. (4) is based on the assumptions that the thickness is equally distributed along any meridian following Jovane's model [24], that the sheet is part of a sphere of radius r and that the volume remains constant during the whole process. This last assumption can be made only if the volume fraction of cavities is negligible [30].

As the strain rate is neither uniform nor constant, a characteristic value will be extracted from the data available from free-inflation tests. More specifically, the characteristic strain-rate associated to a free-inflation test is extracted from the time evolution of the dimensionless height at the centre point of the sample. This evolution usually presents an abrupt transient step during the very first seconds of the tests, where the sample cannot develop any stiffness against a perpendicular gas pressure gradient. After that, a steady growth state, where the slope remains constant, can be observed, Fig. 2.

The strain-rate can be calculated from the dimensionless height evolution [24] as

$$\dot{\varepsilon} = \frac{2H}{1+H^2}\frac{dH}{dt} \tag{5}$$

Being aware that the slope of the dimensionless height versus time curve during the steady growth state has strain-rate dimensions, the characteristic strain-rate is then associated to this slope, $\dot{\varepsilon}_o \approx \dot{H}$. This approximation is justified by observing Fig. 2, in which an aluminium alloy at a single

constant pressure and two different temperatures was tested. Fig. 2a shows the dimensionless height evolution including two straight lines together with the value of the slope. Since these two values have strain-rate dimensions, the straight lines are translated to Fig. 2b as horizontal ones. Applying (5), the strain-rate evolution at the centre point is plotted, where time was normalised with the time needed to reach $H = 1$. Therefore, it is possible to observe that the steady-state slope corresponds to the quasi-constant strain-rate for both tests.

Introducing $\dot{\varepsilon}_o = \dot{H}$ into Eq. (4) and taken into account (2), the apparent viscosity can be calculated as

$$\mu_a = \frac{q_o AR}{4\dot{H}}f(H) \tag{6}$$

This last expression can be simplified if $f(H)$ is plotted and analysed, Fig. 3. Since the steady state was observed to be placed during the second half of the test, that is, $H > 0.5$, the coefficient $f(H)/4$ from Eq. (4) can be replaced by a ω parameter that is lower than 1 and is adjusted using numerical results.

Therefore, Eq. (6) remains

$$\mu_a = \omega \frac{q_o AR}{\dot{H}} \tag{7}$$

The ω parameter from the last equation is estimated applying the estimated K and m into a finite element model and comparing forming time to experimental time from the tests showed in Table 1. Simulated and experimental forming times were measured at $H = 1$ and then calculated the mean of the deviations. For a range of ω between 0.78 and 0.85, the best value is found at 0.80, see Table 1.

Summarising, the steps to obtain K and m parameters from the constitutive power-law function are:

- Measure $H(t)$ from the free-inflation test.
- Assign the constant slope during the steady state of $H(t)$ to the characteristic strain-rate $\dot{\varepsilon}_o$.
- Calculate the apparent viscosity using (7).
- Repeat the process for different $\dot{\varepsilon}_o$ changing q_o.
- Fit $(\dot{\varepsilon}_o, \mu_a)$ pairs with a potential curve to obtain $\mu_a = K\dot{\varepsilon}^{m-1}$.
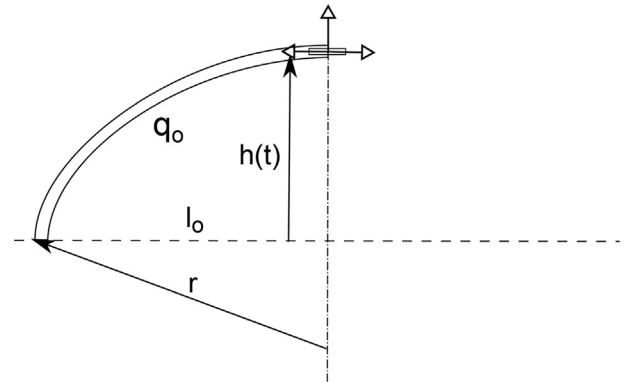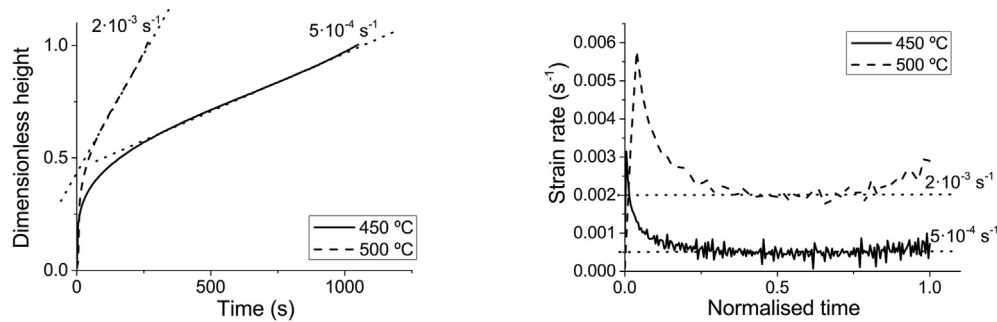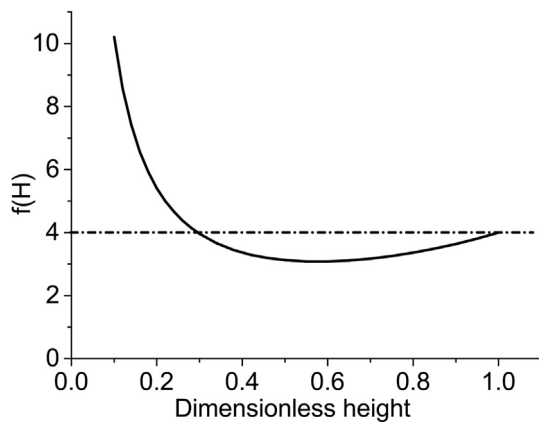

Fig. 1 — Geometric parameters of the test.

Fig. 2 − Alnovi-U alloy tested at 450 °C and 500 °C at 0.60 MPa. (a) Dimensionless height evolution. (b) Strain-rate evolution versus the normalised time.

Fig. 3 − Values for f(H) function from (4).

Table 1 − ω parameters and errors.

ω	0.78	0.79	0.80	0.81	0.82	0.83	0.84	0.85
Error [%]	9.18	7.77	7.12	8.15	7.26	8.79	11.24	11.20

2.2. Experimental procedure

The aforementioned methodology is applied to the tests summarised at Table 2, where information about the material, aspect ratio, forming temperature, external pressure, characteristic strain-rate and forming time (H = 1) is shown. These tests are both extracted from previous works [15,16,28] and performed ad hoc to extend the strain-rate range.

The materials on which the methodology for characterising superplastic behaviour is applied are: a magnesium alloy AZ31 with an average grain size of 11 μm, an aluminum alloy of the 5000 series commercially known as ALNOVI-U, with an average grain size of 8.3 μm, and a titanium alloy Ti−6Al−4V in its 23rd grade (Extreme Low Interstitial).

The tests were performed on a specific experimental apparatus installed on a universal testing machine (INSTRON 4485). The sheet material was interposed between a die and a blank holder embedded in a cylindrical split furnace able to keep the tools and the blank at a constant and uniform temperature.

The clamping force was controlled by the load cell of the universal testing machine. The die had a cylindrical cavity with a 22.5 mm radius and an entry radius of 3 mm. The

furnace temperature was controlled by three thermocouples inserted in the ceramic shell of the furnace in the upper, central and lower zones. The temperature on the material was monitored by a K-type thermocouple that insisted on the dome apex and that was counterbalance by a weight to avoid damaging of the blank that otherwise occurred due to its low strength at high temperatures. The stem of thermocouple went across the entire upper tool (the die) and the crosshead of the testing machine. The metallic upper end of the thermocouple was connected to the cursor of a magnetostrictive position transducer (mounted over the crosshead of the testing machine) by which the current height of the inflated dome could be measured. Argon gas was conveyed by a hole in the blank-holder and acted on the lower surface of the blank. The gas pressure was controlled by an electronic proportional valve. The signals from the thermocouples, the position transducer, the load cell and from the pressure transducer

Table 2 − Tests data. Pressure values in square brackets correspond to test extracted from previous works [15,16,28].

Material/Temp. [ºC]	AR	q_o[MPa]	$\dot{\varepsilon}_o$x10^{-3} [s^{-1}]	t_{exp}[s]
AZ31/450	30	0.2	0.16	3407.2
	30	0.25	0.22	2435.4
	30	0.35	0.45	1185.0
	30	0.5	1.1	422.8
	30	[0.75]	5.99	87
	30	[1.0]	17.6	26
	30	[1.25]	40.5	12
AZ31/520	30	0.11	2.3	2205.5
	30	0.17	4.2	1307.2
Alnovi-U/450	16.7	0.6	0.5	1045.2
	16.7	0.75	0.89	603.3
	16.7	0.9	1.2	435.6
Alnovi/500	16.7	[0.3]	0.22	2499
	16.7	[0.4]	0.47	1190
	16.7	[0.5]	0.82	668.4
	16.7	0.6	2.0	260.4
	16.7	0.7	2.7	199.3
	16.7	0.8	3.2	153.5
Ti−6Al−4V/800	22.5	1.25	0.09	5877.6
	22.5	1.5	0.15	3671.0
	22.5	1.75	0.19	2924.5
Ti−6Al−4V/850	22.5	[0.5]	0.14	4597.5
	22.5	[1.0]	0.36	1815.1
	22.5	[1.5]	0.71	924.3
	22.5	1.75	0.81	711.7
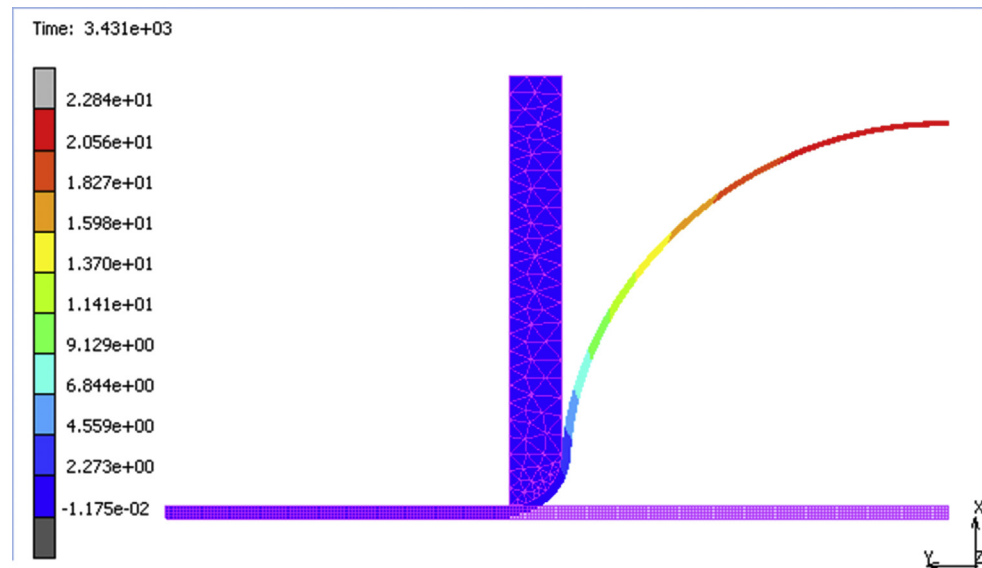
Fig. 4 – Undeformed and fully deformed states of a AZ31 sample at 450 °C and 0.2 MPa Using FEM model. Colour scale corresponds to x displacement.

and the one sent to the proportional valve were managed together on a PC by a Labview® virtual instrument. A scheme of the equipment and further details on the experimental procedure can be found in [28].

2.3.   Numerical model

Experimental forming times are compared with numerical results using an axisymmetric model with **full integration isoparametric** quadrangular elements in the non-linear finite element package MSC.MARC™. Element size is adjusted to obtain four elements along the thickness. **The upper die is modelled using triangular elements and rigid material. Boundary conditions are completed, adding to the axisymmetric conditions, with clamping restrictions over the nodes that are in contact with the blankholder and the corresponding constant pressure over the free face of the sample,** Fig. 4. Moreover, a stop criterion is established to finish the simulation when a displacement equal or greater than 22.5 mm is reached, in which case the test is considered to be completed.

Convergence difficulties were found for values of m lower than 0.3, but they were overcome by increasing the number of recycles of time steps per increment.

3.   Results and discussion

The aforementioned methodology is evaluated in two ways. First, materials from Table 2 are characterised and, from this characterisation, the K and m parameters are inserted into a finite element model in which the simulated forming time is compared with the experimental one. After that, the same methodology is applied to results measured by other authors, where both tensile and biaxial tests are provided. Therefore, the constitutive behaviour from both type of tests can be compared.

3.1.   Forming time estimation

Table 3 shows the list of characterised materials where information on the external pressure is included. The estimation of K and m, according to the methodology explained in the previous section, is compared with the values obtained by applying the methodology of Enikeev and Kruglov [27] (in parentheses). **In the same manner, the last column shows the deviations between the experimental and the simulated forming times, applying the parameters to a FEM model by using both methodologies. In that regard, the forming process is monitored over time for experimental tests and FEM simulations.** Fig. 5 (a) **shows the dimensionless height, H, over t ime while** Fig.5 (b) **shows the calculated strain rates at H, where** Eq. (5) **has been applied**.

The duplication of tests, such as AZ31 at 450 °C at a pressure of 0.35 MPa, means that it has been used in two different test intervals to obtain K and m. A first interval is set from 0.20 to 0.35 MPa, and a second interval from 0.35 to 0.50 MPa. This is so because the interval of tests is established as valid when the strain-rate variation does not exceed 0.5 according to

$$log\frac{\dot{\varepsilon}_n}{\dot{\varepsilon}_1}<0.5 \qquad (8)$$

where the subscript n refers to the last test performed. This criterion is adopted to approximate the $\sigma(\dot{\varepsilon})$ curve by means of a potential function, and it has already been used in other works [14,31] as a criterion for distributing the necessary experimental trials to plot the characteristic curve.

Thus, the set of tests on AZ31 at 450 °C were divided into two intervals in terms of strain rate: one from 1.6×10^{-4} s^{-1} to 4.5×10^{-3} s^{-1}, and the second one between 4.5×10^{-3} s^{-1} and 1.1×10^{-2} s^{-1}. This ensures that Eq. (8) is fulfilled.

In general, a better behaviour is observed by the exposed methodology with respect to the one presented by Enikeev and Kruglov. Compared to an average error of 14.7% for the latter, the average error obtained with the new methodology is

Table 3 — Characterisation of the materials and forming time deviations. Values in parentheses are referred to Enikeev and Kruglov methodology [27].

| Material/Temp. [°C]	q_o[MPa]	K[MPa·s^m]	m	Deviation [%]
AZ31/450	0.2	565.2 (453.2)	0.544 (0.53)	0.7 (−14.8)
	0.25			−6.0 (−23.5)
	0.35			4.3 (−17.8)
	0.35	171.2 (120.9)	0.391 (0.346)	−8.2 (−13.3)
	0.5			3.8 (−13.7)
	[0.75]	70.6 (70.1)	0.267 (0.258)	−23.7 (−11.4)
	[1.0]			−12.7 (−5.0)
AZ31/520	0.11	1126.5 (2091.2)	0.723 (0.832)	10.1 (−22.5)
	0.17			1.9 (−21.3)
Alnovi-U/450	0.6	219.7 (251.9)	0.439 (0.463)	−3.7 (−11.5)
	0.75			−2.0 (−7.0)
	0.9			−9.3 (−12.2)
Alnovi/500	[0.3]	102.1 (103.3)	0.384 (0.387)	−7.2 (−8.8)
	[0.4]			−7.7 (−10.4)
	[0.5]			−8.8 (−9.8)
	0.6	422.2 (209.9)	0.642 (0.544)	2.3 (−12.7)
	0.7			3.5 (−17.5)
	0.8			9.2 (−15.4)
Ti−6Al−4V/800	1.25	782.6 (1860.4)	0.382 (0.482)	−7.9 (−12.7)
	1.5			−8.7 (−3.4)
	1.75			−25.0 (−15.9)
Ti−6Al−4V/850	[0.5]	5074.3 (6251.4)	0.713 (0.746)	−12.4 (−23.5)
	[1.0]			−14.8 (−22.1)
	[1.0]	3676 (2039.6)	0.673 (0.598)	−17.9 (−19.2)
	[1.5]			−8.5 (−19.7)
	1.75			−9.7 (−19.0)
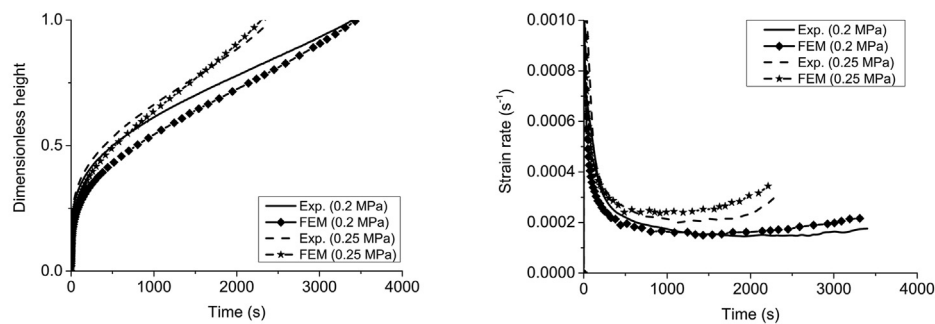
Fig. 5 — Comparison of experimental and FEM tests for AZ31 alloy at 450 °C, 0.2 and 0.25 MPa. (a) Dimensionless height, H, evolution with time. (b) Strain-rate evolution with time at H.

6.7%, where most of the experiments exhibit deviation lower than 10%. Moreover, the error is lower than 5% for half of the tests. The high discrepancy observed in the test on the titanium alloy at 1.75 MPa may come from a change in the behaviour of the material at this strain rate.

The apparent viscosity is graphically showed as a strain-rate dependent function for the three tested materials at the corresponding forming temperatures, see Figs. 6-8. Furthermore, the same methodology is applied to the biaxial tests on the same materials appearing at [15,16,28] respectively, which allow us to obtain a better understanding and a whole constitutive behaviour of these strain-rate dependent materials.

Therefore, three additional tests from [16] on the same batch of AZ31 at 450 °C at 0.75, 1.00 and 1.25 MPa are added to Fig. 6. This additional range was initially divided into two different strain-rate intervals in order to fulfil (8). However,
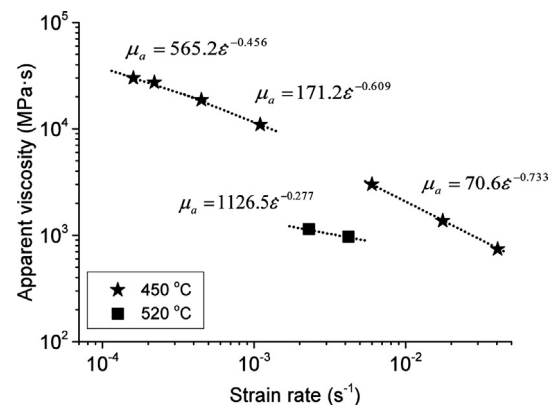
Fig. 6 — Apparent viscosity versus strain-rate for the magnesium alloy AZ31, [16].
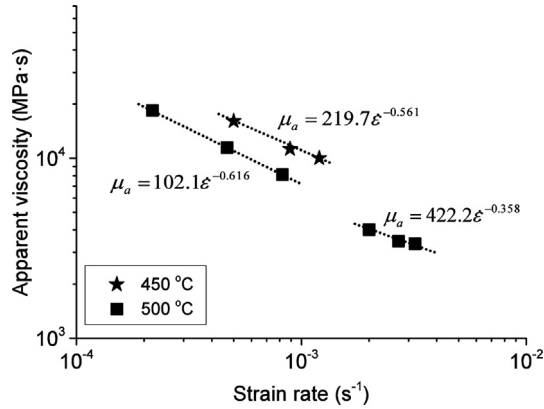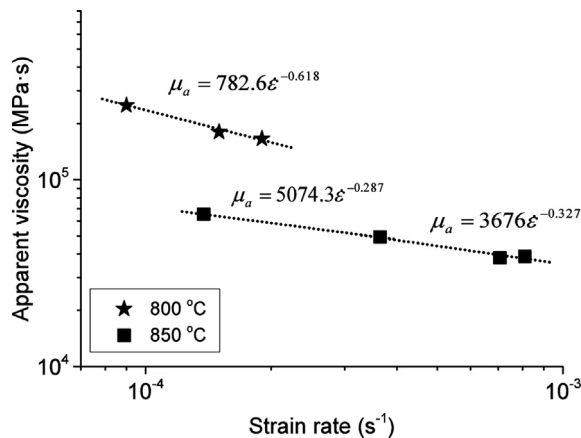
Fig. 7 − Apparent viscosity versus strain-rate for the aluminum alloy Alnovi-U, [15].

the behaviour seems to be quite uniform through the whole strain-rate range and it can be modelled with a single pair of values of $K = 70.6$ MPa·s^m and $m = 0.267$.

Additionally, the Alnovi-U behaviour shown in Fig. 7 is completed by adding the tests for 500 °C at 0.30, 0.40 and 0.50 MPa from [15] over the same batch of material. This new range provides $K = 102.1$ MPa·s^m and $m = 0.384$.

The increase of m at the second strain-rate interval for 500 °C tests might be due to a translation of the optimal strain-rate towards higher values. This is a habitual behaviour when the working temperature is increased [32].

Finally, the apparent viscosity property of the titanium alloy Ti−6Al−4V, Fig. 8, is completed by adding the three tests from [28] at 850 °C at 0.50, 1.00 and 1.50 MPa. Moreover, an additional test at the same temperature was intentionally performed at 1.75 MPa in order to widen this range. These four tests are divided into two different ranges, one from 0.50 to 1.00 MPa, and the second one from 1.00 to 1.75 MPa. The results provide that the two ranges can be modelled using the parameter values ($K = 5074.3$ MPa·s^m, $m = 0.713$) and ($K = 3676$ MPa·s^m, $m = 0.673$) respectively. It is noteworthy that the first pair of values matches with the values ($K = 5229$ MPa· s^m, $m = 0.703$) obtained from the inverse analysis performed at the cited work.

The plots from Figs. 6-8 confirm that the strain-rate dependent functions of the apparent viscosity let us to describe the superplastic materials as members of the subgroup of non-newtonian fluids called pseudoplastic or shear-thinning fluids, which functions can be written as in Eq. (3).

3.2. Constitutive behaviour

As a second evaluation, the same methodology is applied to works from other authors that provide results from tensile and biaxial tests. In this way, using Eq. (2), the methodology can be compared with the constitutive behaviour extracted from the tensile test that follows the standard ASTM E2448-11, [33]. Thus, a total of four different works are analysed: two of them use the same magnesium alloy AZ31 at 450 °C [14,31], and the other two use different aluminium alloys, AA5083 at 450 °C [34], and AMg-6 at 415 °C [26].

It must be mentioned that, in the case where the tensile test provides results for different strains, it is only extracted the result that corresponds to a strain of 0.5. This is because the strain of a semi-meridian ε_m of a completed formed sample, that is $H = 1$, can be calculated as

$$\varepsilon_m = \ln\left(\frac{\frac{\pi l_o}{2}}{l_o}\right) \approx 0.45 \tag{9}$$

Fig. 9 puts together the results from the magnesium alloy AZ31 tests. Thus, the results from [14] are depicted using a solid line to plot the tensile test results. The square symbols represent the values obtained by applying (2), where the apparent viscosity and the strain rate are assessed by following the methodology from section 2. On the other hand, the results from [31] are showed using a dotted line to depict the results from the tensile test, while the circles represents the results from the biaxial tests.

The biaxial and tensile test results from [14] match perfectly, and follow the same curve. The results from [31] are consistent for strain-rate values in the order of 10^{-2} s^{-1}, where

Fig. 8 − Apparent viscosity versus strain-rate for the titanium alloy Ti−6Al−4V, [28].
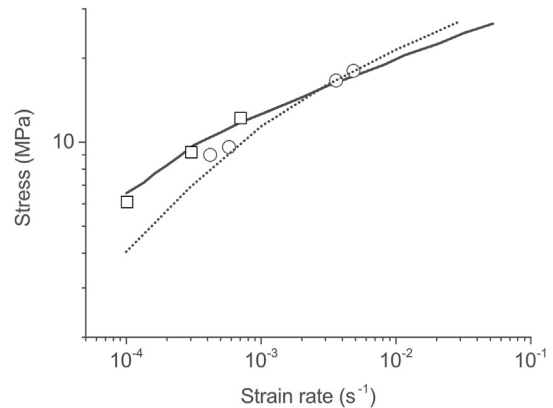
Fig. 9 − Stress vs. strain rate for AZ31 alloys at 450 °C. Solid line and squares refers to tensile and biaxial tests respectively [14]. Dotted line and circles refers to tensile and biaxial tests from [31], respectively.
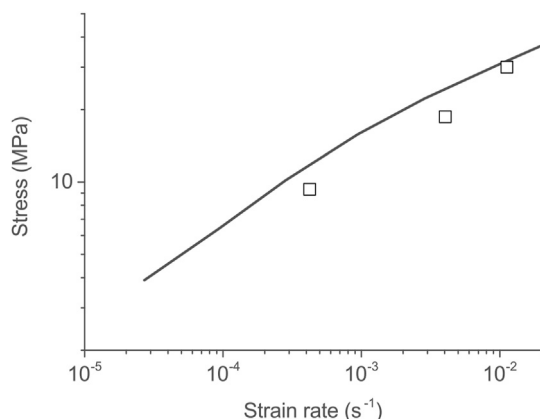
Fig. 10 — Stress vs. strain rate for AA5083 alloy at 450 °C. Solid line and squares refers to tensile and biaxial tests respectively [34].

a good match is found. For lower strain rates, in the order of 10^{-3} s^{-1}, the deviation increases to 10%.

Results on the aluminium alloy AA5083 are showed in Fig. 10, where the solid line correspond to the results from the tensile test and the square symbols from the biaxial tests obtained at 0.45, 0.83 and 0.90 MPa. These results differ in the order of the 20% for the results at 4×10^{-4} and 4×10^{-3} s^{-1} respect to the results from the tensile tests. This difference reduces to 3% for the biaxial test performed at 0.90 MPa.

Finally, Fig. 11 compares the results from five biaxial tests on the aluminium alloy AMg-6 at 0.30, 0.35, 0.40, 0.50 and 0.60 MPa, and the analytical viscoplastic behaviour model from Smirnov [35] for long ranges of strain rates.

$$\sigma = \sigma_s \frac{\sigma_o + k_v \dot{\varepsilon}^{m_v}}{\sigma_s + k_v \dot{\varepsilon}^{m_v}} \qquad (10)$$

where σ_o is a threshold stress, σ_s is a yield stress, and k_v and m_v are material parameters.

Following the same pattern, the solid line corresponds to the analytical model and the square symbols to the biaxial
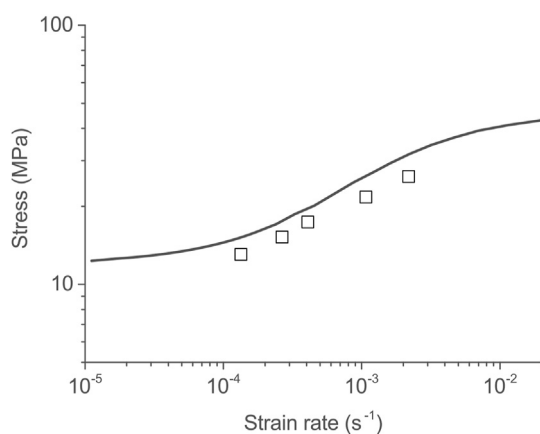
Fig. 11 — Stress vs. strain rate for AMg-6 alloy at 415 °C. Solid line and squares refers to viscoplastic model and biaxial tests respectively [26].

tests. In that sense, it is observed that the results from the biaxial tests underestimate the stress function in the order of a 15% respect to the viscoplastic model.

4.   Conclusions

This work presents a new straight-forward methodology to characterise the superplastic behaviour parameters of materials. The methodology makes use of free-inflation tests, in which the height evolution at the centre point of a blank sheet is measured. The material is characterised by a function called apparent viscosity that reveals the strain-rate dependence behaviour and classifies superplastic materials as members of the shear-thinning non-newtonian fluids group.

The methodology is applied on three superplastic alloys carrying out new *ad-hoc* tests and collecting others from the literature. The validity of the methodology is checked in two different ways: firstly, by comparing the deviation of the simulated forming times from the experimental ones by the presented methodology and the one followed by Enikeev and Kruglov; secondly, by comparing stress vs. strain-rate curves constructed by applying uniaxial tests and also by the new methodology, which is based on biaxial tests.

Results show that the obtained superplastic parameters are in the order of those assessed by the Enikeev and Kruglov's method, and that the latter ones provide better results once they are used in a finite element software. Moreover, the results obtained with the new methodology fit well with the behaviour shown using the standardised uniaxial test, opening the door to a new standardisation of the characterisation of superplastic materials by using free-inflation tests.

Declaration of Competing Interest

The authors declare that they have no known competing financial interests or personal relationships that could have appeared to influence the work reported in this paper.

Acknowledgements

REFERENCES

[1] Barnes AJ. Superplastic forming 40 Years and still growing. J Mater Eng Perform 2007;16:440—54. https://doi.org/10.1007/s11665-007-9076-5.

[2] Langdon TG. Seventy-five years of superplasticity: historic developments and new opportunities. J Mater Sci 2009;44:5998—6010. https://doi.org/10.1007/s10853-009-3780-5.

[3] Han W, Zhang K, Wang G. Superplastic forming and diffusion bonding for honeycomb structure of Ti-6Al-4V alloy. J Mater

Process Technol 2007;183:450—4. https://doi.org/10.1016/j.jmatprotec.2006.10.041.

[4] Lee KS, Huh H. Simulation of superplastic forming/diffusion bonding with finite-element analysis using the convective coordinate system. J Mater Process Technol 1999;89—90:92—8. https://doi.org/10.1016/S0924-0136(99)00051-5.

[5] Lee KS, Huh H. Numerical simulation of the superplastic moving die forming process with a modified membrane finite element method. J Mater Process Technol 2001;113:754—60. https://doi.org/10.1016/S0924-0136(01)00706-3.

[6] Carrino L, Giuliano G, Palmieri C. On the optimisation of superplastic forming processes by the finite-element method. J Mater Process Technol 2003;143:373—7. https://doi.org/10.1016/S0924-0136(03)00423-0.

[7] Bonet J, Gil A, Wood RD, Said R, Curtis RV. Simulating superplastic forming. Comput Methods Appl Mech Eng 2006;195:6580—603. https://doi.org/10.1016/j.cma.2005.03.012.

[8] Chumachenko EN. Development of computer simulation of industrial superplastic sheet forming. Mater Sci Eng, A 2009;499:342—6. https://doi.org/10.1016/j.msea.2007.11.129.

[9] Giuliano G, Franchitti S. The determination of material parameters from superplastic free-bulging tests at constant pressure. Int J Mach Tools Manuf 2008;48:1519—22. https://doi.org/10.1016/j.ijmachtools.2008.05.007.

[10] Albakri M, Abu-Farha F, Khraisheh M. A new combinded experimental-numerical approach to evaluate formability of rate dependent materials. Int J Mech Sci 2013;66:55—66. https://doi.org/10.1016/j.ijmecsci.2012.10.008.

[11] Yoo JT, Yoon JH, Lee HS, Youn SK. Material characterization of Inconel 718 from free bulging test at high temperature. J Mech Sci Technol 2012;26:2101—5. https://doi.org/10.1007/s12206-012-0523-3.

[12] Luckey SG, Friedman PA, Weinmann KJ. Correlation of finite element analysis to superplastic forming experiments. J Mater Process Technol 2007;194:30—7. https://doi.org/10.1016/j.jmatprotec.2007.03.122.

[13] Kim YH, Hong SS, Lee JS, Wagoner RH. Analysis of superplastic forming processes using a finite-element method. J Mater Process Technol 1996;62:90—9.

[14] Carpenter AJ, Antoniswamy AR, Carter JT, Hector LG, Taleff EM. A mechanism-dependent material model for the effects of grain growth and anisotropy on plastic deformation of magnesium alloy AZ31 sheet at 450 °C. Acta Mater 2014;68:254—66. https://doi.org/10.1016/j.actamat.2014.01.043.

[15] Sorgente D, Tricarico L. Characterization of a superplastic aluminium alloy ALNOVI-U through free inflation tests and inverse analysis. Int J Mater Form 2014;7:179—87. https://doi.org/10.1007/s12289-012-1118-3.

[16] Sorgente D, Palumbo G, Scintilla LD, Tricarico L. Gas forming of an AZ31 magnesium alloy at elevated strain rates. Int J Adv Manuf Technol 2016;83:861—72. https://doi.org/10.1007/s00170-015-7614-0.

[17] Yoon JH, Yi YM, Lee HS. Material characterization of duplex stainless steel by superplastic free bulging test. Mater Werkst 2012;43:805—9. https://doi.org/10.1002/mawe.201200046.

[18] Frary M, Schuh C, Dunand DC. Kinetics of biaxial dome formation by transformation superplasticity of titanium alloys and composites. Metall Mater Trans 2002;33:1669—80. https://doi.org/10.1007/s11661-002-0176-4.

[19] Franchitti S, Giuliano G, Palumbo G, Sorgente D, Tricarico L. On the optimisation of superplastic free forming test of an AZ31 magnesium alloy sheet. Int J Mater Form 2008;1:1067—70. https://doi.org/10.1007/s12289-008-0.

[20] Jarrar FS, Abu-Farha FK, Hector Jr LG, Khraisheh MK. Simulation of high-temperature aa5083 bulge forming with a hardening/softening material model. J Mater Eng Perform 2009;18:863—70. https://doi.org/10.1007/s11665-008-9322-5.

[21] Antoniswamy AR, Taleff EM, Hector Jr LG, Carter JT. Plastic deformation and ductility of magnesium AZ31B-H24 alloy sheet from 22 to 450 °C. Mater Sci Eng, A 2015;631:1—9. https://doi.org/10.1016/j.msea.2015.02.018.

[22] Pradeep S, Pancholi V. Superplastic forming of multipass friction stir processed aluminum-magnesium alloy. Metall Mater Trans A 2014;45:6207—16. https://doi.org/10.1007/s11661-014-2573-x.

[23] ASTM. E2712-15: standard test methods for bulge-forming superplastic metallic sheet. ASTM; 2015.

[24] Jovane F. An approximate analysis of the superplastic forming of a thin circular diaphragm: theory and experiments. Int J Mech Sci 1968;10:403—27.

[25] Belk JA. A quantitative model of the blow-forming of spherical surfaces in superplastic sheet metal. Int J Mech Sci 1975;17:505—11. https://doi.org/10.1016/0020-7403(75)90015-6.

[26] Aksenov SA, Chumachenko EN, Kolesnikov AV, Osipov SA. Determination of optimal gas forming conditions from free bulging tests at constant pressure. J Mater Process Technol 2015;217:158—64. https://doi.org/10.1016/j.jmatprotec.2014.11.015.

[27] Enikeev FU, Kruglov AA. An analysis of the superplastic forming of a thin circular diaphragm. Int J Mech Sci 1995;37:473—83.

[28] Sorgente D, Palumbo G, Piccininni A, Guglielmi P, Tricarico L. Modelling the superplastic behaviour of the Ti6Al4V-ELI by means of a numerical/experimental approach. Int J Adv Manuf Technol 2017;90. https://doi.org/10.1007/s00170-016-9235-7.

[29] Majidi O, Jahazi M, Bombardier N. A viscoplastic model based on a variable strain rate sensitivity index for superplastic sheet metals. Int J Mater Form 2019;12:693—702. https://doi.org/10.1007/s12289-018-1443-2.

[30] Majidi O, Jahazi M, Bombardier N. Prediction of material behavior during biaxial stretching of superplastic 5083 aluminum alloy. Int J Adv Manuf Technol 2019;102:2357—66.

[31] Taleff EM, Hector Jr LG, Verma R, Krajewski PE, Chang JK. Material models for simulation of superplastic Mg alloy sheet forming. J Mater Eng Perform 2010;19:488—94. https://doi.org/10.1007/s11665-010-9612-6.

[32] Alabort E, Putman D, Reed RC. Superplasticity in Ti-6Al-4V: characterisation, modelling and applications. Acta Mater 2015;95:428—42. https://doi.org/10.1016/j.actamat.2015.04.056.

[33] ASTM. E2448-11: standard test method for determining the superplastic properties of metallic sheet materials. ASTM; 2011.

[34] Taleff EM, Hector Jr LG, Bradley JR, Verma R, Krajewski PE. The effect of stress state on high-temperature deformation of fine-grained aluminum — magnesium alloy AA5083 sheet. Acta Mater 2009;57:2812—22. https://doi.org/10.1016/j.actamat.2009.02.036.

[35] Smirnov OM. Metal working in a superplastic state. Mashinostryenie (in Russ 1979)